Advanced Steel Construction – Vol. 22 No. 1 (2026) 116–129
DOI:10.18057/IJASC.2026.22.1.10

EFFICIENT CROSS-SECTIONAL ANALYSIS TECHNIQUE FOR ARBITRARY-SHAPED STEEL SECTIONS USING GAUSSIAN SEGMENTAL ELEMENTS

Wen-Long Gao [1], Liang Chen [1, *], A.H.A. Abdelrahman [2] and Si-Wei Liu [1]

[1] *Department of Civil and Environmental Engineering, The Hong Kong Polytechnic University, Hung Hom, Kowloon, Hong Kong, China*

[2] *Department of Structural Engineering, Faculty of Engineering, Mansoura University, Egypt*

** (Corresponding author: E-mail: liang17.chen@connect.polyu.hk)*

ABSTRACT

This research introduces an efficient cross-sectional analysis algorithm utilizing innovative Gaussian segmental elements for arbitrary-shaped steel sections. Steel members with arbitrary-shaped sections are gradually widely employed in engineering due to their mechanical benefits. Achieving accuracy in cross-sectional analysis remains crucial for the understanding of their comprehensive structural behavior and enhancing design optimization. Traditional fiber-based cross-sectional analysis methods prioritize accuracy but often compromise computational efficiency. The proposed algorithm leverages the Gaussian quadrature method, renowned for its precise approximation of definite integrals, to address complex cross-sectional geometries. In addition, a refined line-segment model is introduced to solve the overlapping problem by configuring eccentricities at the ends of segments. The paper elaborates on the derivation of the novel Gaussian segmental element designed for modeling the arbitrary-shaped section, determining the section properties, generating full yield surfaces, and calculating the moment-thrust-curvature relationships. Notably, the algorithm balances accuracy and computational efficiency by strategically selecting integration Gauss points and weights across thicknesses. Three groups of examples are provided to demonstrate the accuracy and efficiency of the proposed method for the cross-sectional analysis of arbitrary-shaped steel sections.

ARTICLE HISTORY

Received: 06 November 2025
Revised: 26 January 2026
Accepted: 6 February 2026

KEYWORDS

Arbitrary-shaped steel sections;
Cross-sectional analysis;
Yield surface;
Moment-thrust-curvature;
Gauss integration

1. Introduction

Steel members with arbitrary-shaped sections are gradually widely used in contemporary steel constructions due to their elevated flexibility forms and structural efficacy. In addition, robotic welding machines and building information modeling eliminate the constraints of fabricating such sections. Accurate and efficient cross-sectional analysis of the arbitrary-shaped sections is crucial in understanding their mechanical behavior and optimizing their design for practice design. One widely employed approach is the fiber-based method, which facilitates the analysis of complex cross-sectional geometries and material properties, allowing for a comprehensive investigation of essential parameters like cross-section properties [1-5], full yield surface [6-8], and moment-curvature relationships [9-11].

Accurate calculations of cross-sectional properties are vital for analyzing and designing members with arbitrary-shaped steel sections. Researchers have thoroughly explored various techniques for calculating cross-sectional properties encompassing torsional, shear, and nonsymmetrical section properties [12-14]. For example, Waldron [1] introduced the sectorial method of analysis, emphasizing its potential to incorporate warping restraint effects for torsional analysis in thin-walled beams. However, complexities in calculating sectorial functions hindered its applicability. Expanding this discourse, Chai Hong and Acra [2] delved into torsional and flexural properties of multicellular cross-sections, proposing an algorithm to tackle indeterminate shear flows and thus analyze sections with complex geometries. Li et al. [3] introduced a numerical procedure for analyzing arbitrary beam-columns, accounting for residual stresses and geometric imperfections, crucial in designing high-strength steel structures. Shortly after, Bourihane et al. [15] developed a beam-column element for stability analyses of beams comprising thin-walled open sections under various loading conditions. Elkaimbillah et al. [16] extended this research and proposed a refined beam-column element for the nonlinear dynamic behavior of thin-walled open-section composite beams. Hancock and Rasmussen [17, 18] further analyzed members with nonsymmetrical cross-sections accounting for the misalignment between the cross-sectional centroid and shear center. More recently, Chen et al. [19] introduced an efficient line-element method for second-order analysis of steel members with nonsymmetrical thick-walled sections, addressing twisting effects and warping degrees of freedom alongside a two-dimensional finite-element cross-section analysis method implemented in the educational software MASTAN2 [20]. While these studies offer significant insights, limitations persist. Challenges remain in analyzing sections with complex geometries or substantial torsion.

Notably, cross-sectional analysis for arbitrary-shaped steel sections has seen notable advancements, particularly in understanding their yield capacity and section properties. The concept of the yield surface, encompassing axial force and bending responses, plays a pivotal role in determining section behavior [21-24]. While conventional methodologies, such as the one proposed by McGuire et al. [6], have provided valuable insights for symmetric sections, addressing nonsymmetrical shapes remains challenging. Nonsymmetrical sections are extensively used for their structural efficiency, necessitating accurate analysis techniques. In this context, the approach proposed by Liu et al. [7] introduces a cross-section analysis method that calculates yield surfaces for both symmetric and nonsymmetrical sections. This method harnesses the Quasi-Newton divergence-free algorithm and integrates the fiber-based model. More recently, Chen et al. [8] developed an improved line-element formulation to model nonsymmetrical sections' geometric and material nonlinear behaviors. The proposed methodology not only generates yield surfaces of arbitrary steel sections but also employs gradients for effective plastic flow control. However, it is acknowledged that the complexities associated with generating the fiber model may introduce challenges in terms of applicability for complex geometries and computational efficiency.

The moment-thrust-curvature relationships of steel sections offer crucial insights into their structural behavior under bending. These relationships illuminate how the sections respond to axial load and bending moments, thereby effectively guiding engineers in designing and analyzing these components [25-30]. Duan et al. [9] examined the moment-curvature relationships for dented tubular sections under combined biaxial bending and axial load. Their work introduced closed-form moment-thrust-curvature expressions for dented and undented tubular sections. Additionally, Liew et al. [10] extended the concept of moment-thrust-curvature relationships to address inelastic and geometrically non-linear structural problems involving elements subjected to combined axial load and bending. Their numerical discretized cross-section method yielded moment-thrust-curvature relationships for I-sections, rectangular box-sections, and circular or elliptical hollow sections. Exploring moment-thrust-curvature relationships enriches the broader investigation into the cross-sectional analysis, complementing the studies on yield surfaces, cross-sectional properties, and section capacity checks.

Generally, the previous studies predominantly focused on symmetric sections and often implemented the time-consuming fiber-based models. To fill the research gap, this paper presents a novel algorithm for precisely determining cross-section properties, the full yield surface, and the moment-thrust-curvature of the cross-sections. The proposed algorithm leverages the Gaussian quadrature method, renowned for its precise approximation of definite integrals [31-36], to address complex cross-sectional geometries. Additionally, a refined Coordinate Method was introduced to eliminate the interaction between the adjacent elements in the line-segment model by configuring eccentricities at the ends of segments. The paper elaborates on the derivation of the novel Gaussian segmental element (GSE) and provides three groups of examples to demonstrate the accuracy and efficiency of the proposed GSE for the cross-sectional analysis of arbitrary-shaped steel sections.

2. Cross-section modeling using gaussian segmental element

The fiber-based approach is widely used for cross-sectional analysis [3, 7, 8, 11, 19], where full section meshing or excessive fiber generation is required to obtain the accurate section properties, yield surfaces, or the moment-curvature. Despite its utility, the fiber-based approach introduces its own set of challenges, notably the intricate fiber mesh generation algorithm. This algorithm necessitates extensive effort to ascertain the number of fibers and their geometric details, such as center coordinates and area, thus complicating the process of building and meshing sections. Addressing these challenges, an innovative cross-sectional modeling and analysis methodology using GSE is developed in this paper, offering an efficient alternative to conventional fiber-based models.

2.1. Gaussian segmental element

This study introduces a novel method employing the GSE based on the line finite element method, aiming to enhance the efficiency and accuracy of cross-sectional analysis. The Gaussian integration strategy is applied for area integration in the cross-sectional plane, offering a better balance between computational cost and accuracy compared to the classical 2D finite element method, which uses a fiber section obtained from meshing the geometric model. The cross-sectional configuration is generated using a line-segment approach, consisting of a series of segments and points, as illustrated in Fig. 1(b). Each segment is aligned with the central axis of the section plate and is defined by two points representing its start and end. These segments are not only defined by the two points but are also associated with the thickness of the section plate.

Furthermore, the initially established global axis system, denoted as *Z-O-Y*, determines each point's coordinates, with Gaussian points systematically distributed along the section's thickness and length based on the integral range (Fig. 1c). In this research, a GSE has three columns of Gauss integral points along the section plate thickness and seven rows of Gauss integral points along its length.

The distribution of Gauss points directly governs the integration accuracy of the proposed GSE. With Gauss–Legendre quadrature, increasing the number of Gauss points enhances the order of accuracy for evaluating sectional integrals, allowing accurate results with far fewer sampling points than uniform fiber partitioning. In the present study, three Gauss points through the thickness and seven Gauss points along the segment length are adopted as a practical balance between accuracy and efficiency for thin-walled steel sections, where the through-thickness stress variation is typically mild under the adopted sectional assumptions. For problems involving sharper stress gradients (e.g., locally thick regions, pronounced nonlinearity localization, or refined residual-stress patterns), accuracy can be further improved by increasing the Gauss points and/or refining the line-segment representation, analogous to mesh refinement in fiber-based models.

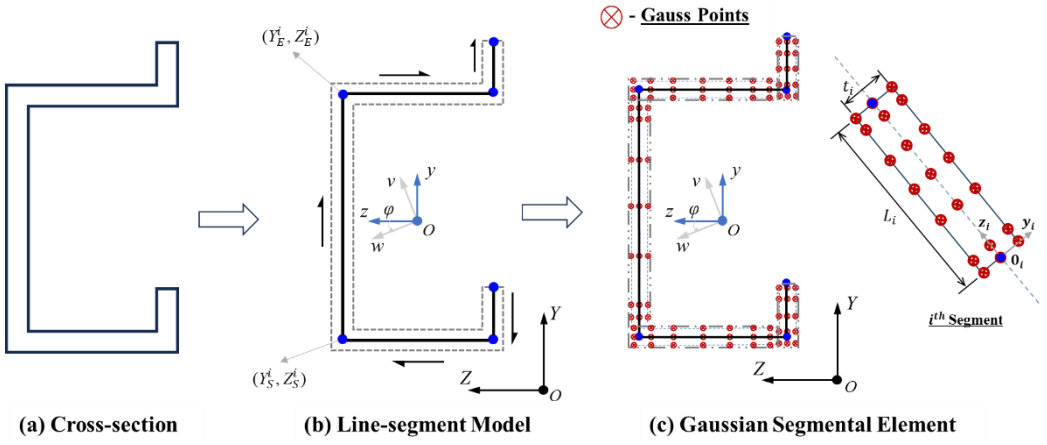

Fig. 1 Cross-section modeling using the Gaussian line-segment approach

A local axis system denoted as *zi-oi-yi* is established to obtain the distribution of Gauss points in each segment, as depicted in Fig. 1 (c), in which three Gauss points are distributed along the thickness, and seven Gauss points along the length of each segment. This distribution configuration of Gauss points in a segment is both efficient and sufficient for most common cases. In extreme cases, such as when the segment is too thin or too thick, the distribution of Gauss points can be automatically adjusted based on the width-to-thickness ratio. The coordinates of each Gauss integration point within its respective local axis system are determined by the following equations:

$$y^i_{m,n} = \xi^i_{m,n} t_i \qquad (m = 1 \sim 3, n = 1 \sim 7) \tag{1}$$

$$z^i_{m,n} = \zeta^i_{m,n} L_i \qquad (m = 1 \sim 3, n = 1 \sim 7) \tag{2}$$

where the subscripts m and n represent the m^{th} and n^{th} Gauss points in the section plate's thickness and length directions. The coefficients, $\xi^i_{m,n}$ and $\zeta^i_{m,n}$, representing the location of Gauss points distributed on each segment in two directions, should vary for each segment due to its length-to-thickness ratio. t_i and L_i denote the thickness and length of the i^{th} segment in the line-segment model, respectively. The locations and the weight factors for the Gauss points used in this research are given in Tables 1 and 2.

Table 1
The locations and weight factors of Gauss points in the thickness direction

Gauss point m	1	2	3
$\xi^i_{m,n}$	-0.387298	0	0.387298
H_m	0.277778	0.444444	0.277778

Table 2
The location and weight factors of Gauss points in the length direction

Gauss point n	1	2	3	4	5	6	7
$\zeta^i_{m,n}$	0.02545	0.12923	0.29708	0.5	0.70292	0.87077	0.97455
H_n	0.06474	0.13985	0.19092	0.20897	0.19092	0.13985	0.06474

2.2. Refined line-segment model with eccentricity at segment ends

Modeling tree-type sections like I-sections and T-sections using the line-segment approach poses a challenge in the conventional Coordinate Method [37], primarily due to overlapping areas between the flange and the web. A refined line-segment model is introduced to solve the problem by configuring eccentricities at the ends of segments as shown in Fig. 2. Eccentricities e^i_S and e^i_E, are introduced at the start and end of segment i (defined in the local z_i-o_i-y_i system) to eliminate overlap between intersecting plates (e.g., flange–web intersection). The sign of e^i_S and e^i_E follows the local axis convention (as illustrated, $e^s_i < 0$ and $e^e_i > 0$). The updated segment ending coordinates are obtained using Eqs. (3)–(6).

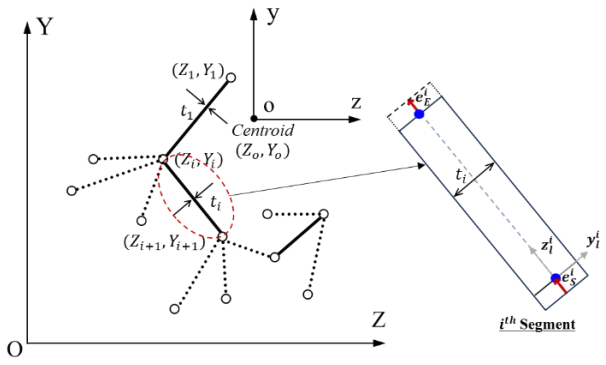

Fig. 2 Refined line-segment model with end eccentricities

The updated geometrical information of points and segments of the improved line-segment model can be obtained by following expressions.

$$Ye_E^i = \lambda_i e_E^i + Y_E^i \tag{3}$$

$$Ze_E^i = \mu_i e_E^i + Z_E^i \tag{4}$$

$$Ye_S^i = \lambda_i e_S^i + Y_S^i \tag{5}$$

$$Ze_E^i = \mu_i e_S^i + Z_S^i \tag{6}$$

where, Y_S^i, Z_S^i, Y_E^i and Z_E^i are used to define the start and end point coordinates of the i^{th} segment, as per the global axis system. These values represent the positioning of the points before considering the eccentricities. In addition, $\lambda_i = \frac{Y_E^i - Y_S^i}{L_i}$ and $\mu_i = \frac{Z_E^i - Z_S^i}{L_i}$ represent the projections of the length L_i in the horizontal and vertical directions, respectively.

2.3. Differences between the fiber-based section modeling and GSE section modeling

The proposed GSE section modeling streamlines geometry input by requiring only point coordinates, segment thickness, and relevant connection details. This simplification allows for the rapid creation of analysis models, circumventing complex modeling procedures. Conversely, the fiber-based model necessitates a more intricate approach that begins with the creation of an outline for the actual section by detailing coordinates of each corner point and loop information to form a closed geometric shape, followed by the implementation of a mesh algorithm to generate numerous fibers, each requiring the recording of centroid coordinates and cross-sectional area for analysis. The fiber-based method can be particularly cumbersome and time-consuming, especially when dealing with complex cross-sections. The proposed method eliminates the need for fiber meshing by employing a limited number of Gauss points to accelerate the procedure of the cross-sectional analysis.

From a numerical perspective, both the fiber-based model and the proposed GSE aim to evaluate the same sectional integrals (e.g., axial force, bending moments, and section properties) by sampling stress/strain over the cross-sectional area. The key difference lies in the sampling and integration strategy. The fiber-based method discretizes the cross-section into a large number of small area patches (fibers) and typically performs summation using low-order quadrature (often equivalent to midpoint/rectangular integration), such that accuracy improves primarily by increasing the number of fibers. In contrast, the proposed GSE represents each plate component by a line segment with an associated thickness and evaluates the sectional integrals using Gauss–Legendre quadrature points and weights distributed in the thickness and length directions of each segment. This strategy can achieve high integration accuracy with substantially fewer evaluation points, thereby improving computational efficiency while preserving accuracy for thin-walled steel sections.

3. Cross-sectional analysis using gse

3.1. Sectional property calculation

In arbitrary-shaped steel sections, the principal coordinate system of the cross-section, represented as the *w-o-v* axis in Fig. 1, is essential, especially for the nonsymmetrical sections [20]. This system incorporates an inclined angle, symbolized as φ, which determines the orientation between the geometric *y-o-z* coordinate system and the principal *w-o-v* coordinate system. The angle φ can be computed using the expression outlined below, which plays a crucial role in accurately defining the cross-sectional geometry.

$$\varphi = \frac{1}{2}\arctan\left(\frac{2I_{yz}}{I_y - I_z}\right) \tag{7}$$

in which, I_y, I_z and I_{yz} represent the cross-section moment of inertia along the respective axes. These values are crucial for understanding the stiffness properties of the arbitrary-shaped steel sections and can be calculated using the following equations:

$$\begin{aligned} I_z &= \int y^2 dA \\ &\doteq \frac{1}{3}\sum_{i=1}^{Ns} A_i\left(\left(Ye_S^i - Y_c\right)^2 + \left(Ye_S^i - Y_c\right)\left(Ye_E^i - Y_c\right) + \left(Ye_E^i - Y_c\right)^2\right) + \frac{1}{3}\sum_{i=1}^{Ns} A_{is}\left(\frac{t_i^2}{4}\mu_i^2\right) \\ &= \sum_{i=1}^{Ns}\frac{A_i}{3}\left(y_S^i y_S^i + y_S^i y_E^i + y_E^i y_E^i + \frac{t_i^2}{4}\mu_i^2\right) + \sum_{i=1}^{Ns}\lambda_i\frac{A_i}{3}\left(e_S^i e_S^i\lambda_i + e_E^i e_E^i\lambda_i + e_S^i e_E^i\lambda_i + 2y_S^i e_S^i + y_S^i e_E^i + y_E^i e_S^i + 2y_E^i e_E^i\right) \end{aligned} \tag{8}$$

$$\begin{aligned} I_y &= \int z^2 dA \\ &\doteq \frac{1}{3}\sum_{i=1}^{Ns} A_i\left(\left(Ze_S^i - Z_c\right)^2 + \left(Ze_S^i - Z_c\right)\left(Ze_E^i - Z_c\right) + \left(Ze_E^i - Z_c\right)^2\right) + \frac{1}{3}\sum_{i=1}^{Ns} A_i\left(\frac{t_i^2}{4}\lambda_i^2\right) \\ &= \sum_{i=1}^{Ns}\frac{A_i}{3}\left(z_S^i z_S^i + z_S^i z_E^i + z_E^i z_E^i + \frac{t_i^2}{4}\lambda_i^2\right) + \sum_{i=1}^{Ns}\lambda_i\frac{A_i}{3}\left(e_S^i e_S^i\mu_i + e_E^i e_E^i\mu_i + e_S^i e_E^i\mu_i + 2z_S^i e_S^i + z_S^i e_E^i + z_E^i e_S^i + 2z_E^i e_E^i\right) \end{aligned} \tag{9}$$

$$\begin{aligned} I_{yz} &= \int yz dA \\ &\doteq \frac{1}{6}\sum_{i=1}^{Ns} A_i\begin{pmatrix} 2\left(Ze_S^i - Z_c\right)\left(Ye_S^i - Y_c\right) + \left(Ze_S^i - Z_c\right)\left(Ye_E^i - Y_c\right) \\ + \left(Ze_E^i - Z_c\right)\left(Ye_S^i - Y_c\right) + 2\left(Ze_E^i - Z_c\right)\left(Ye_E^i - Y_c\right) \end{pmatrix} + \frac{1}{6}\sum_{i=1}^{Ns} A_i\left(\frac{t_i^2}{2}\lambda_i\mu_i\right) \\ &= \sum_{i=1}^{Ns}\frac{A_i}{6}\left(2z_S^i y_S^i + z_S^i y_E^i + z_E^i y_S^i + 2z_E^i y_E^i\right) + \sum_{i=1}^{Ns}\frac{A_i}{6}\left(\frac{t_i^2}{2}\lambda_i\mu_i\right) \\ &+ \sum_{i=1}^{Ns}\lambda_i\frac{A_i}{6}\left(2\lambda_i\mu_i\left(e_S^i + e_E^i\right)^2 + \left(\mu_i y_S^i + \lambda_i z_S^i\right)\left(2e_S^i + e_E^i\right) + \left(\mu_i y_E^i + \lambda_i z_E^i\right)\left(e_S^i + 2e_E^i\right)\right) \end{aligned} \tag{10}$$

where, N_s stands for the number of segments and A_i is the area of the i^{th} segment. Y_c and Z_c are the centroidal coordinates of the cross-section. The equations consider the eccentricities at both ends of each segment and the thickness of the section plate, overcoming the overlapping areas between the flange and the web in the conventional Coordinate Method. The inclusion of additional eccentricities in these calculations significantly improves the accuracy and

versatility in assessing the properties of various steel sections. It is important to note that the calculations for the warping constant and torsional constant in this study rely on the thin-walled assumption. Detailed expressions for these section properties can be found in the referenced literatures [20, 38].

3.2. Yield surface generation

In this research, the GSE is adapted to generate the full yield surface of the arbitrary-shaped steel sections to improve the computational efficiency. In accordance with the Euler-Bernoulli hypothesis, there is a linear strain distribution along the vertical direction of the entire section, as illustrated in Fig. 3. For strains within the elastic limit, the strain-stress relationship remains linear, permitting the use of Hooke's Law for stress determination. However, when strain exceeds the elastic limit, stress must be calculated using the material's specific strain-stress curve. The full yield surface of the arbitrary-shaped steel sections referring to the principal axis system *w-o-v* can be effectively determined using equations derived for the GSE, offering a viable alternative to the fiber model.

$$P_x = \int_A f_s(\varepsilon)dA = \int_w \int_v f_s(\varepsilon)dwdv = \sum_{i=1}^{Ns}\sum_{m=1}^{3}\sum_{n=1}^{7} H_m t_i H_n L_i f_s(\varepsilon_{m,n}^i) \tag{11}$$

$$M_w = \int_A f_s(\varepsilon)(v-v_n)dA = \int_w \int_v f_s(\varepsilon)(v-v_n)dwdv = \sum_{i=1}^{Ns}\sum_{m=1}^{3}\sum_{n=1}^{7} H_m t_i H_n L_i f_s(\varepsilon_{m,n}^i)(v_{m,n}^i - v_n) \tag{12}$$

$$M_v = \int_A f_s(\varepsilon)(w-w_n)dA = \int_w \int_v f_s(\varepsilon)(w-w_n)dwdv = \sum_{i=1}^{Ns}\sum_{m=1}^{3}\sum_{n=1}^{7} H_m t_i H_n L_i f_s(\varepsilon_{m,n}^i)(w_{m,n}^i - w_n) \tag{13}$$

in which, P_x, M_v and M_w represent the ultimate axial and bending capacities of the section, respectively; $f_s(\varepsilon)$ denotes the stress-strain relationship for the material. v_n and w_n denote the coordinates of the neutral axis in the *v-o-w* axis system; $v_{m,n}^i$ and $w_{m,n}^i$ are the coordinates of the Gauss point situated in the m^{th} row and n^{th} column on the i^{th} segment, and $\varepsilon_{m,n}^i$ represents the strain at the corresponding Gauss point, which can be determined using the following calculation:

$$\varepsilon_{m,n}^i = \varepsilon_u d_{m,n}^i / d_n \tag{14}$$

in which, ε_u represents the ultimate strain at the topmost part of the entire section; d_n is the depth of the neutral axis, as shown in Fig. 3, under a specified axial load level.

To acquire the data points of the full-yield surface, the interactive curve of M_v versus M_w under varying axial loads P_a will be calculated, ranging from minimum to maximum axial strengths. This process involves rotating the inclined angle between the principal axis and the neutral axis from 0 to 2π. In this context, the ultimate strain ε_u in the vertical direction is assumed to be the edge yield strain. The depth of the neutral axis, d_n, can be determined using the Quasi-Newton algorithm.

$$d_n^{k+1} = d_L^{k+1} + \frac{d_U^k - d_L^k}{P_U^k - P_L^k}\left(P_a - P_L^k\right) \tag{15}$$

in which, d_n^{k+1} represents the depth of the neutral axis in the subsequent iteration. d_U^k and d_L^k denote the depths of the neutral axis when the axial strengths are less than and greater than P_a, respectively. P_U^k and P_L^k denote the axial resistances calculated using d_U^k and d_L^k. Upon determining the depth of the neutral axis under a specified axial load, one data point of the full yield surface can be obtained through Eqs. (9)-(11).

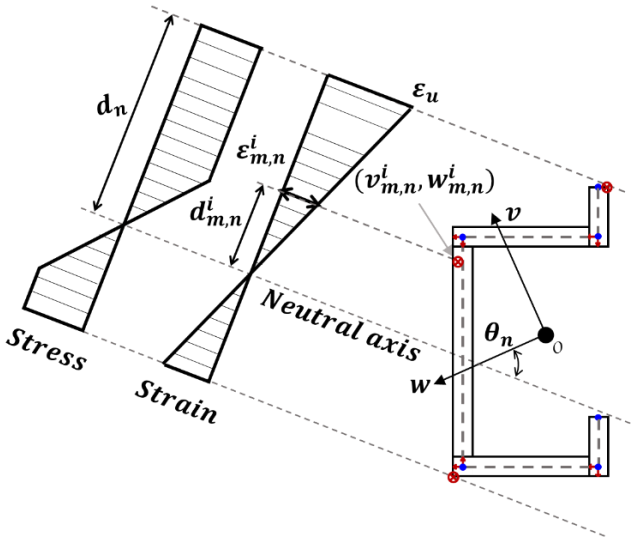

Fig. 3 Assumed strain/stress distribution for yield-surface generation

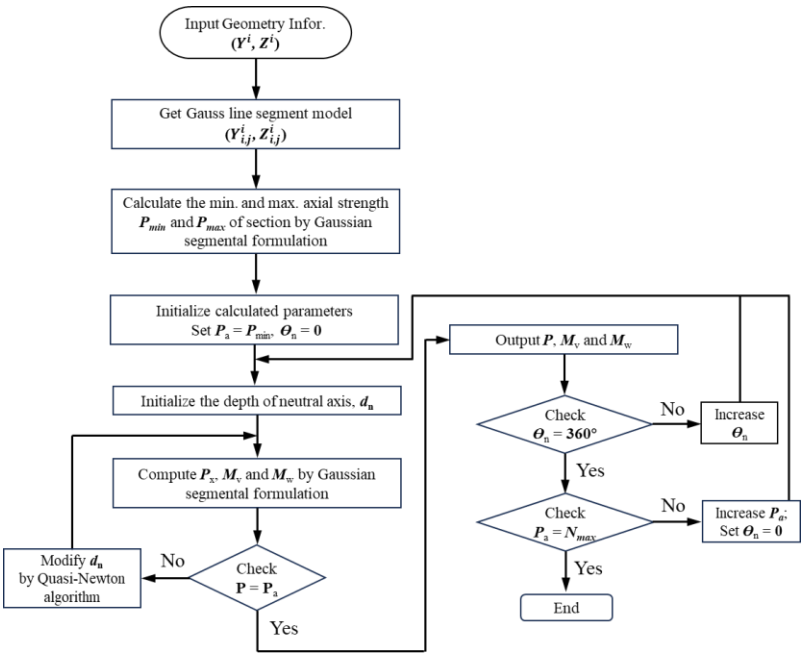

Fig. 4 Flowchart of the full-yield surface generation by Gaussian line-segment model

The analysis flowchart for generating the full yield surface using the GSE formulation is depicted in Fig. 4, successfully implemented in MSASect2 [39]. As shown in the flowchart, the analysis begins with inputting basic geometric data, such as the coordinates of points in the line-segment model. Following this, the Gaussian line-segment model, as proposed in this study, is employed, obviating the necessity for mesh generation. The minimum (tension) and maximum (compression) axial capacities of the section will be subsequently calculated.

Following this, and based on the axial load step setting, the initial axial load P_a is set as the minimum axial capacity. At this axial load level, the inclined angle of the neutral axis, θ_n changes from 0 to 2π. The section's moment capacities (M_v and M_w) are then calculated at each angle. This procedure is repeated for various axial load levels, incrementally increasing from the minimum to the maximum axial capacity. By conducting these calculations, a series of data points are generated, which collectively create the complete yield surface for the arbitrary-shaped steel sections.

3.3. Moment-thrust-curvature calculation

For the moment-thrust-curvatures analysis using the GSE formulation, a combination of the displacement-based method and the Quasi-Newton approach is utilized in the incremental and iterative procedures. The process begins by determining the axial strain of the section under a given axial load. Subsequently, the strain at the extreme Gauss point of the Gaussian line-segment model is incrementally increased until the ultimate strength is reached. Concurrently, the location of the neutral axis is ascertained at each strain increment, enabling the calculation of the corresponding curvature and moment resistance. The initial axial strain of the section under axial load P_a can be calculated using the following iterative procedure.

$$\varepsilon_n^{k+1} = \varepsilon_L^{k+1} + \frac{\varepsilon_U^k - \varepsilon_L^k}{P_U^k - P_L^k}\left(P_a - P_L^k\right) \tag{16}$$

where, ε_n^{k+1} represents the strain of the section at the next iterative step. ε_L^k and ε_U^k are the strains from the previous iterative step, with the resistances being less and more than the applied axial load P_a, respectively.

Additionally, a similar iteration algorithm can be utilized to compute the location of the neutral axis, d_n, as per Eq. (13). Following this, the moment resistance of the section can be determined using the stress integration method, as expressed in Eqs. (10) or (11), while applying the Gauss segmental formulation. The corresponding curvature of the section can be calculated using the following formula.

$$\phi^i = \varepsilon_T^i / d_n^i \tag{17}$$

in which, ε_T^i represents the strain of the section top at the i^{th} moment step, which increments from the initial strain ε_a under the applied axial load P_a to the ultimate strain of steel. Utilizing the incremental procedure, the complete moment versus curvature curve under the applied axial load P_a can be obtained.

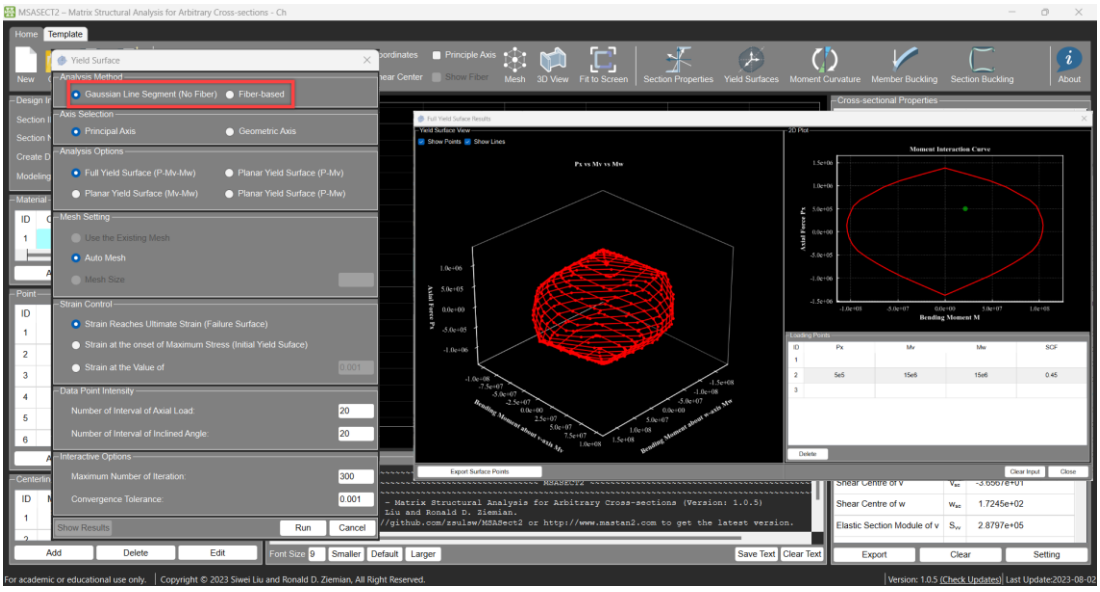

Fig. 5 Yield surface module in MSASect2 [39]

4. Numerical implementation

The cross-sectional analyses approach using the GSE has been effectively integrated into the educational cross-sectional analysis software MSASect2 [39]. Developed by the second author in collaboration with their team, this software is equipped with robust analysis features. These include assessments of cross-sectional properties, yield surfaces, moment-thrust-curvature relationships, member buckling strength, and section buckling strength. With the incorporation of the GSE formulations, MSASect2 [39] now facilitates more extensive analyses and comparative studies. Fig. 5 showcases the software's user-friendly interface, specifically designed for the yield surface function. It allows users to choose between the traditional fiber-based method and the Proposed GSE approach. This interface significantly enhances the practicality of MSASect2 [39], empowering users to efficiently compare and assess different methodologies for analyzing yield surfaces.

5. Validation examples

This section presents three sets of examples to demonstrate the accuracy and efficiency of the proposed method using GSE for the cross-sectional analysis of arbitrary-shaped steel sections. Section properties, yield surfaces, and moment-thrust-curvature curves for several arbitrary-shaped steel sections are calculated and compared with those from the fiber-based model. All computational times reported in this paper were measured on a Dell Precision 3660 workstation (Windows 11 Home, Version 10.0.22631 Build 22631; Intel Core i9-12900K, 16 cores/24 threads, 3.2 GHz base), and both the fiber-based and GSE-based models were executed under identical software settings to ensure a fair comparison.

5.1. Example 1 – Validation of section properties calculation

In this example, the proposed GSE is employed to calculate various geometrical properties for arbitrary-shaped sections with open- and closed-section shapes. While basic cross-sectional properties such as area (A), moments of inertia about geometrical axes (I_y and I_z), warping constant (I_ω), and torsional rigidity (J), are usually straightforward to be calculated, advanced geometrical properties mainly related to nonsymmetrical sections (i.e., Wagner coefficients, β_v, β_w and β_ω as well as the shear center coordinates Y_S and Z_S) are crucial and require further consideration. Accordingly, four sectional shapes, as shown in Fig. 6, are analyzed to show the reliability of the proposed algorithm.

Tables 3-6 present comparisons between the results obtained from the present study and those from the fiber-based model (benchmarks) and traditional Coordinate Method [37]. The proposed algorithm demonstrates

reliability and efficiency, as it yields almost identical results for all section types compared to the fiber-based model with much less computational time. In addition, the proposed method can calculate the basic cross-sectional properties such as area (A) and moments of inertia about geometrical axes (I_y and I_z) more accurately compares to the traditional Coordinate Method.

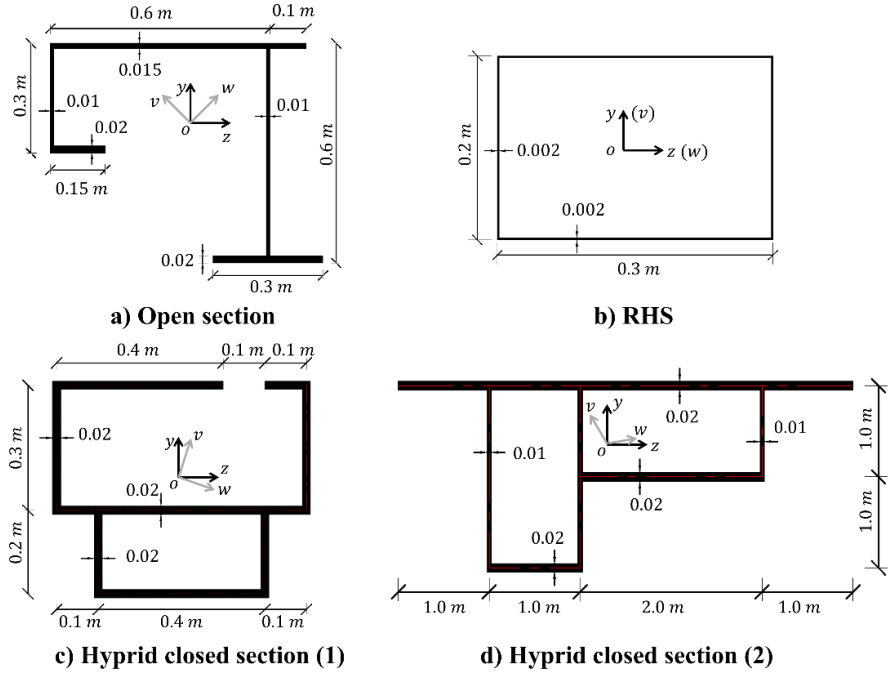

Fig. 6 Schematic diagram of cross-section shapes investigated

Table 3
Section properties for section a

Parameter	Fiber-based model	Coordinate Method	Diff.	Present Study	Diff.
Computational time (sec.)	0.91	Less than 0.01	-	Less than 0.01	-
$\boldsymbol{A}$ (m^2)	2.833E-02	2.850E-02	0.60%	2.832E-02	0.04%
$\boldsymbol{I_y}$ (m^4)	1.772E-03	1.779E-03	0.40%	1.772E-03	0.00%
$\boldsymbol{I_z}$ (m^4)	1.625E-03	1.642E-03	1.05%	1.627E-03	-0.12%
$\boldsymbol{J}$ (m^4)	2.278E-06	2.288E-06	0.44%	2.281E-06	-0.13%
$\boldsymbol{I_w}$ (m^6)	9.246E-05	9.258E-05	0.13%	9.258E-05	-0.13%
$\boldsymbol{Y_s}$ (m)	4.232E-01	4.232E-01	0.00%	4.232E-01	0.00%
$\boldsymbol{Z_s}$ (m)	-1.161E-01	-1.161E-01	0.00%	-1.162E-01	-0.09%
$\boldsymbol{\phi}$	4.189E+01	4.211E+01	0.53%	4.210E+01	-0.50%
$\boldsymbol{\beta_v}$ (m)	-4.370E-01	-4.390E-01	0.46%	-4.387E-01	-0.39%
$\boldsymbol{\beta_w}$ (m)	9.290E-01	9.280E-01	-0.11%	9.282E-01	0.09%
$\boldsymbol{\beta_\omega}$	-1.065E-01	-1.059E-01	-0.56%	-1.058E-01	0.66%

Table 4
Section properties for section b

Parameter	Fiber-based model	Coordinate Method	Diff.	Present Study	Diff.
Computational time (sec.)	0.25	Less than 0.01	-	Less than 0.01	-
$\boldsymbol{A}$ (m^2)	1.984E-03	1.984E-03	0.00%	1.984E-03	0.00%
$\boldsymbol{I_y}$ (m^4)	2.641E-05	2.640E-05	-0.04%	2.640E-05	-0.04%
$\boldsymbol{I_z}$ (m^4)	1.427E-05	1.427E-05	0.00%	1.427E-05	0.00%
$\boldsymbol{J}$ (m^4)	2.823E-05	2.808E-05	-0.53%	2.812E-05	-0.39%
$\boldsymbol{I_w}$ (m^6)	5.984E-09	5.849E-09	-2.26%	5.889E-09	-1.59%
$\boldsymbol{Y_s}$ (m)	0.0	0.0	-	0.0	-
$\boldsymbol{Z_s}$ (m)	0.0	0.0	-	0.0	-
$\boldsymbol{\phi}$	0.0	0.0	-	0.0	-
$\boldsymbol{\beta_v}$ (m)	0.0	0.0	-	0.0	-
$\boldsymbol{\beta_w}$ (m)	0.0	0.0	-	0.0	-
$\boldsymbol{\beta_\omega}$	0.0	0.0	-	0.0	-

Table 5
Section properties for section c

Parameter	Fiber-based model	Coordinate Method	Diff.	Present Study	Diff.
Computational time (sec.)	0.09	Less than 0.01	-	Less than 0.01	-
$\boldsymbol{A}$ (m^2)	4.960E-02	5.000E-02	0.81%	4.960E-02	0.00%
$\boldsymbol{I_y}$ (m^4)	2.166E-03	2.179E-03	0.60%	2.178E-03	0.55%
$\boldsymbol{I_z}$ (m^4)	1.573E-03	1.572E-03	-0.06%	1.571E-03	-0.13%
$\boldsymbol{J}$ (m^4)	4.491E-04	4.333E-04	-3.52%	4.330E-04	-3.58%
$\boldsymbol{I_w}$ (m^6)	1.823E-04	1.812E-04	-0.60%	1.812E-04	-0.60%
$\boldsymbol{Y_s}$ (m)	-2.741E-01	-2.741E-01	0.00%	-2.742E-01	0.04%
$\boldsymbol{Z_s}$ (m)	1.674E-01	1.674E-01	0.00%	1.675E-01	0.06%
$\boldsymbol{\phi}$	-7.000E+00	-7.000E+00	0.00%	-6.997E+00	-0.04%
$\boldsymbol{\beta_v}$ (m)	-2.659E-01	-2.680E-01	0.79%	-2.682E-01	0.86%
$\boldsymbol{\beta_w}$ (m)	-6.778E-01	-6.732E-01	-0.68%	-6.734E-01	-0.65%
$\boldsymbol{\beta_\omega}$	1.543E-01	1.535E-01	-0.52%	1.535E-01	-0.52%

Table 6
Section properties for section d

Parameter	Fiber-based model	Coordinate Method	Diff.	Present Study	Diff.
Computational time (sec.)	0.92	Less than 0.01	-	Less than 0.01	-
$\boldsymbol{A}$ (m^2)	2.096E-01	2.100E-01	0.19%	2.096E-01	0.00%
$\boldsymbol{I_y}$ (m^4)	3.224E-01	3.229E-01	0.16%	3.228E-01	0.12%
$\boldsymbol{I_z}$ (m^4)	1.022E-01	1.023E-01	0.10%	1.023E-01	0.10%
$\boldsymbol{J}$ (m^4)	9.265E-02	9.265E-02	0.00%	9.265E-02	0.00%
$\boldsymbol{I_w}$ (m^6)	1.333E-02	1.333E-02	0.00%	1.333E-02	0.00%
$\boldsymbol{Y_s}$ (m)	1.570E-01	1.571E-01	0.06%	1.571E-01	0.06%
$\boldsymbol{Z_s}$ (m)	-3.660E-01	-3.660E-01	0.00%	-3.660E-01	0.00%
$\boldsymbol{\phi}$	8.058E+01	8.058E+01	0.00%	8.058E+01	0.00%
$\boldsymbol{\beta_v}$ (m)	7.978E-01	7.910E-01	-0.85%	7.930E-01	-0.60%
$\boldsymbol{\beta_w}$ (m)	2.896E-01	2.935E-01	1.35%	2.932E-01	1.24%
$\boldsymbol{\beta_\omega}$	-1.762E+00	-1.775E+00	0.74%	-1.775E+00	0.74%

5.2. Example 2 – Validation of yield surface generation

This example presents an evaluation of the proposed method for generating yield surfaces for arbitrary-shaped steel sections, as illustrated in Fig. 7. Four sections are considered: an L-section, a T-section, a lipped channel section, and an irregular open section. These sections are modelled using the proposed method GSE, in which three and seven Gauss points are used along the thickness and length direction of a segment. The yield curves (i.e., p-m_y, p-m_z, m_z-m_y, p-m_v, p-m_w, and m_v-m_w) are plotted in Figs. 8-11, with y-z and v-w representing the geometric and principal axes, respectively. For comparison purposes, the results from the fiber-based cross-sectional analysis method [8] and equations given by ANSI/AISC-360-16 [30] and McGuire et al. [6] are also provided.

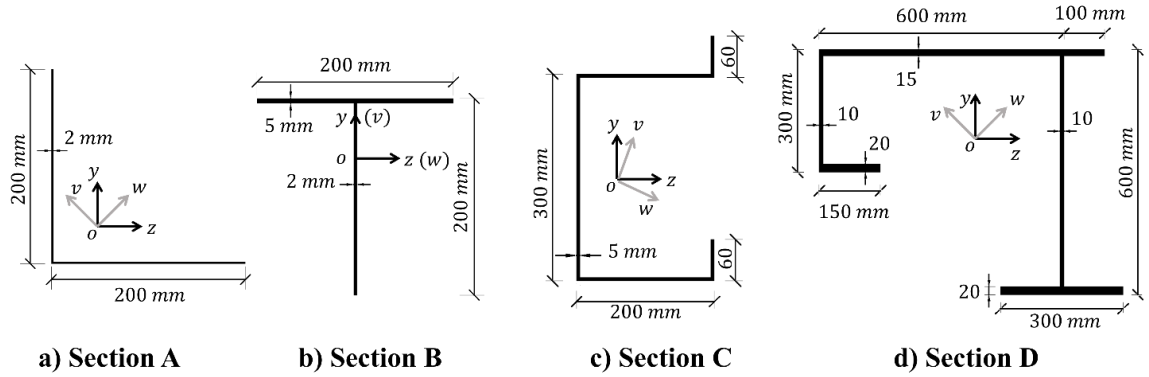

Fig. 7 Typical nonsymmetrical sections for generation of yield surface

The results presented in Figs. 8-11 show that the proposed algorithm can accurately generate yield surfaces that closely match those obtained from the advanced fiber-based model [8]. This demonstrates that the commonly used number of Gauss points for integration is sufficient and that further increasing the number of Gauss points, with additional computational effort, can yield more convergent results. Notably, the proposed method obtains these results with significantly reduced computational time compared to the fiber-based model. From a practical standpoint, reduced computational time is most beneficial when yield surfaces must be generated repeatedly, such as in parametric studies of arbitrary/built-up sections, design iterations and optimization, or when assessing multiple member types within a project. Although the time saving for a single section may appear modest in absolute terms, the computational benefit accumulates quickly when the yield surface is sampled over many axial-load levels and neutral-axis orientations. The

consistent time reductions observed in the validation studies (e.g., Table 7 for moment–thrust–curvature calculations) indicate that the proposed approach can improve analysis throughput without compromising accuracy.

Conversely, the calculation methods proposed by ANSI/AISC-360-16 [30] and McGuire et al. [6] are not suitable for analyzing nonsymmetrical sections. The former relies on conservative linear interaction curves for the yield surface, which tends to fall inside the precisely generated yield surface. Meanwhile, the equation provided by McGuire et al. [6] occasionally overestimates section capacities, as illustrated in Fig. 8 for equal leg angle sections.

Based on the findings presented in Figs. 8-11, this example provides additional evidence supporting the efficiency and reliability of the proposed method for modeling nonsymmetrical sections and accurately generating their yield surfaces. In contrast, existing calculation methods, such as those described in ANSI/AISC-360-16 [31] and McGuire et al. [6], are insufficient when dealing with arbitrary-shaped steel sections. The results obtained from the proposed method provide further evidence of its accuracy and computational efficiency over these existing methods, further highlighting the importance of employing more advanced and specialized techniques for accurate analysis of yield surfaces in such cases.

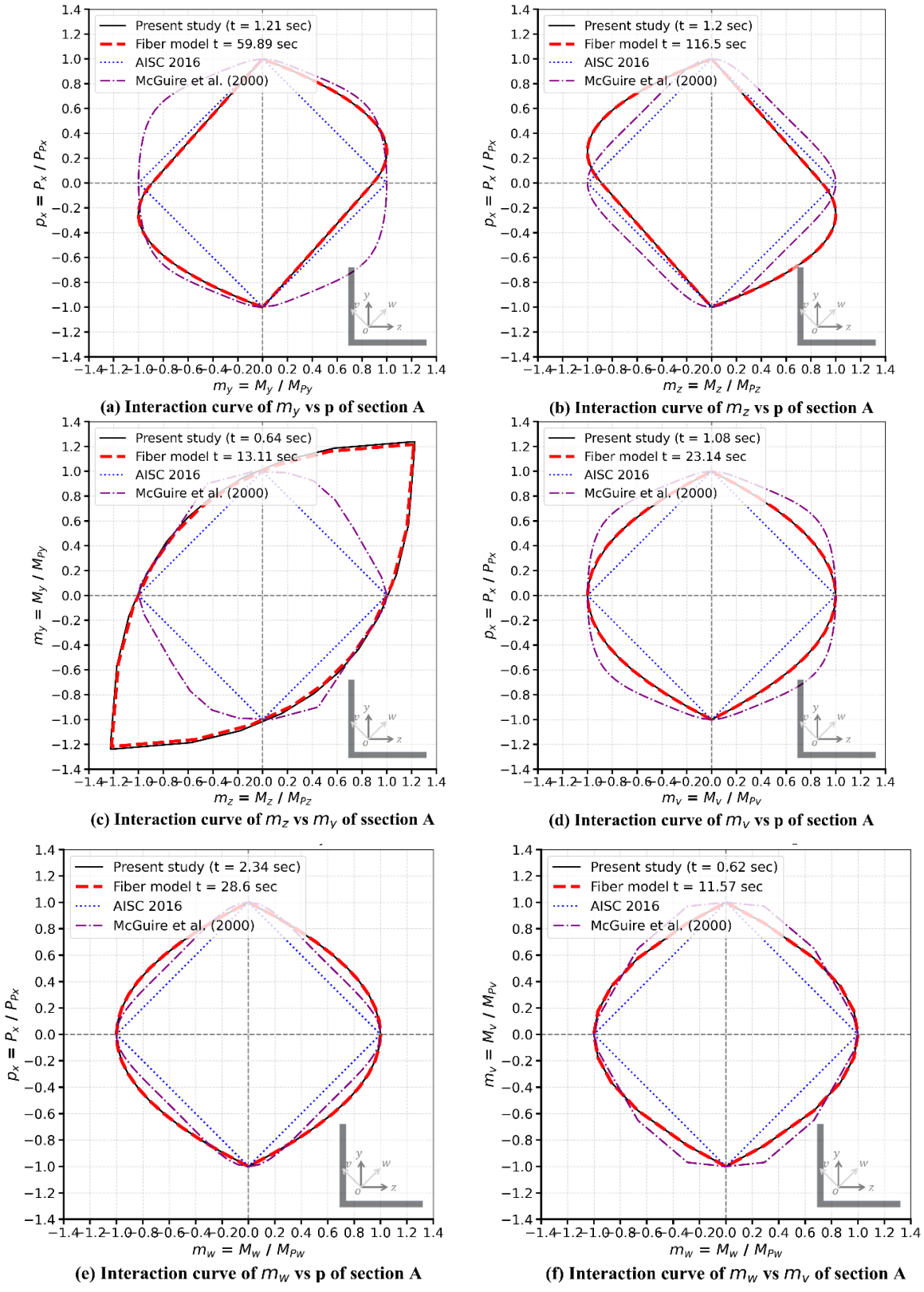

(a) Interaction curve of m_y vs p of section A

(b) Interaction curve of m_z vs p of section A

(c) Interaction curve of m_z vs m_y of ssection A

(d) Interaction curve of m_v vs p of section A

(e) Interaction curve of m_w vs p of section A

(f) Interaction curve of m_w vs m_v of section A

Fig. 8 Comparison results for the yield surface of section A

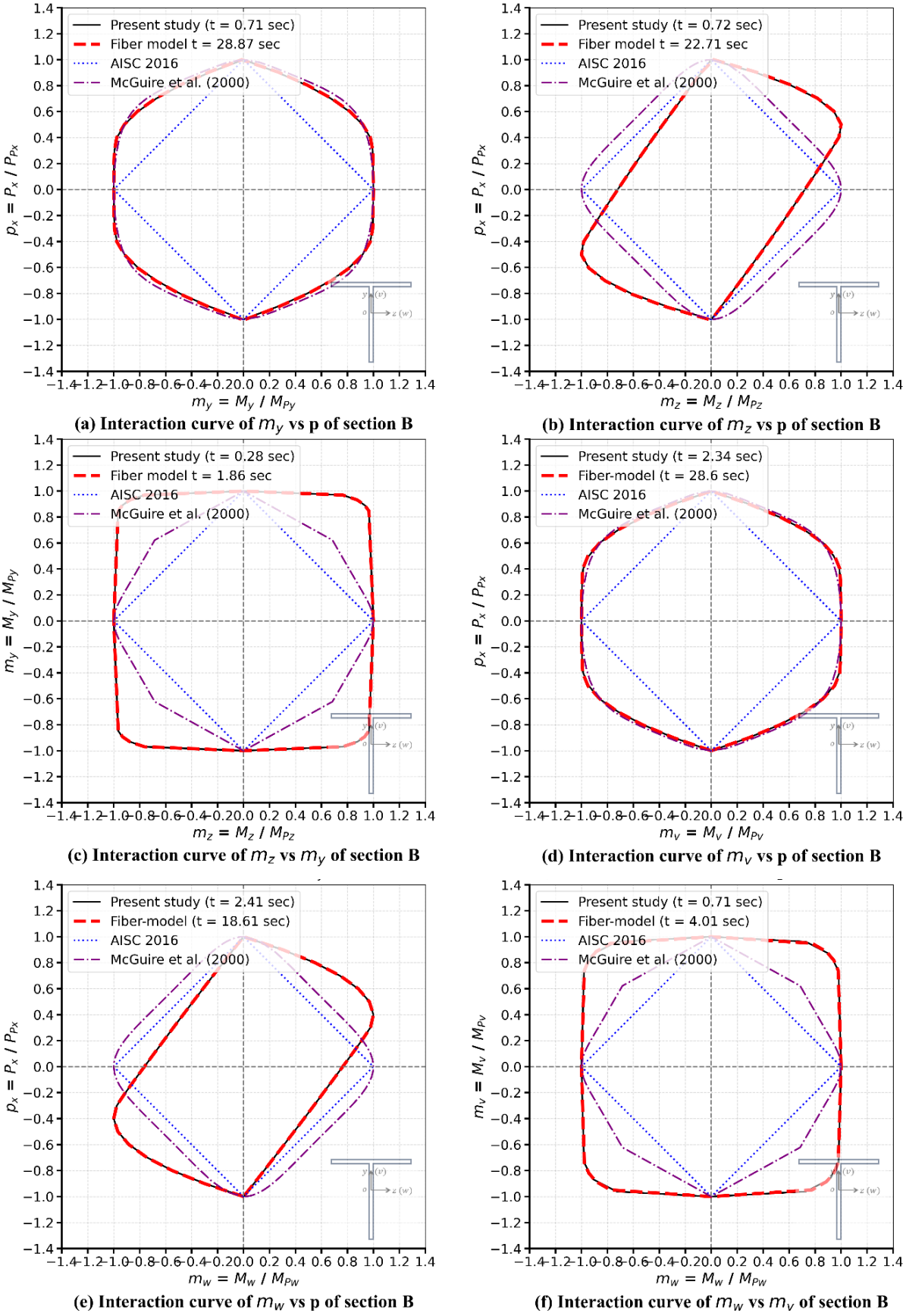

(a) Interaction curve of m_y vs p of section B

(b) Interaction curve of m_z vs p of section B

(c) Interaction curve of m_z vs m_y of section B

(d) Interaction curve of m_v vs p of section B

(e) Interaction curve of m_w vs p of section B

(f) Interaction curve of m_w vs m_v of section B

Fig. 9 Comparison results for the yield surface of section B

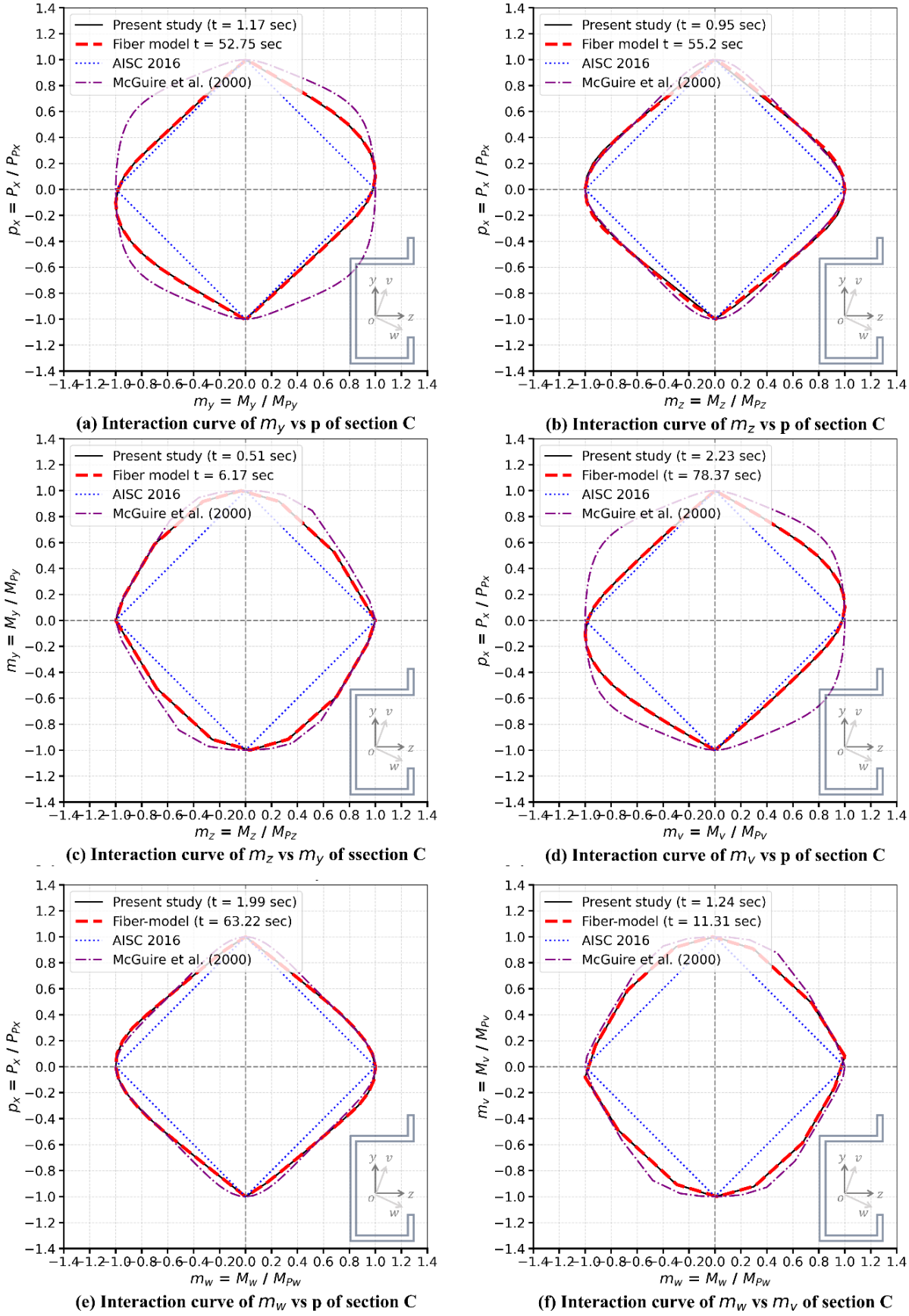

(a) Interaction curve of m_y vs p of section C

(b) Interaction curve of m_z vs p of section C

(c) Interaction curve of m_z vs m_y of ssection C

(d) Interaction curve of m_v vs p of section C

(e) Interaction curve of m_w vs p of section C

(f) Interaction curve of m_w vs m_v of section C

Fig. 10 Comparison results for the yield surface of section C

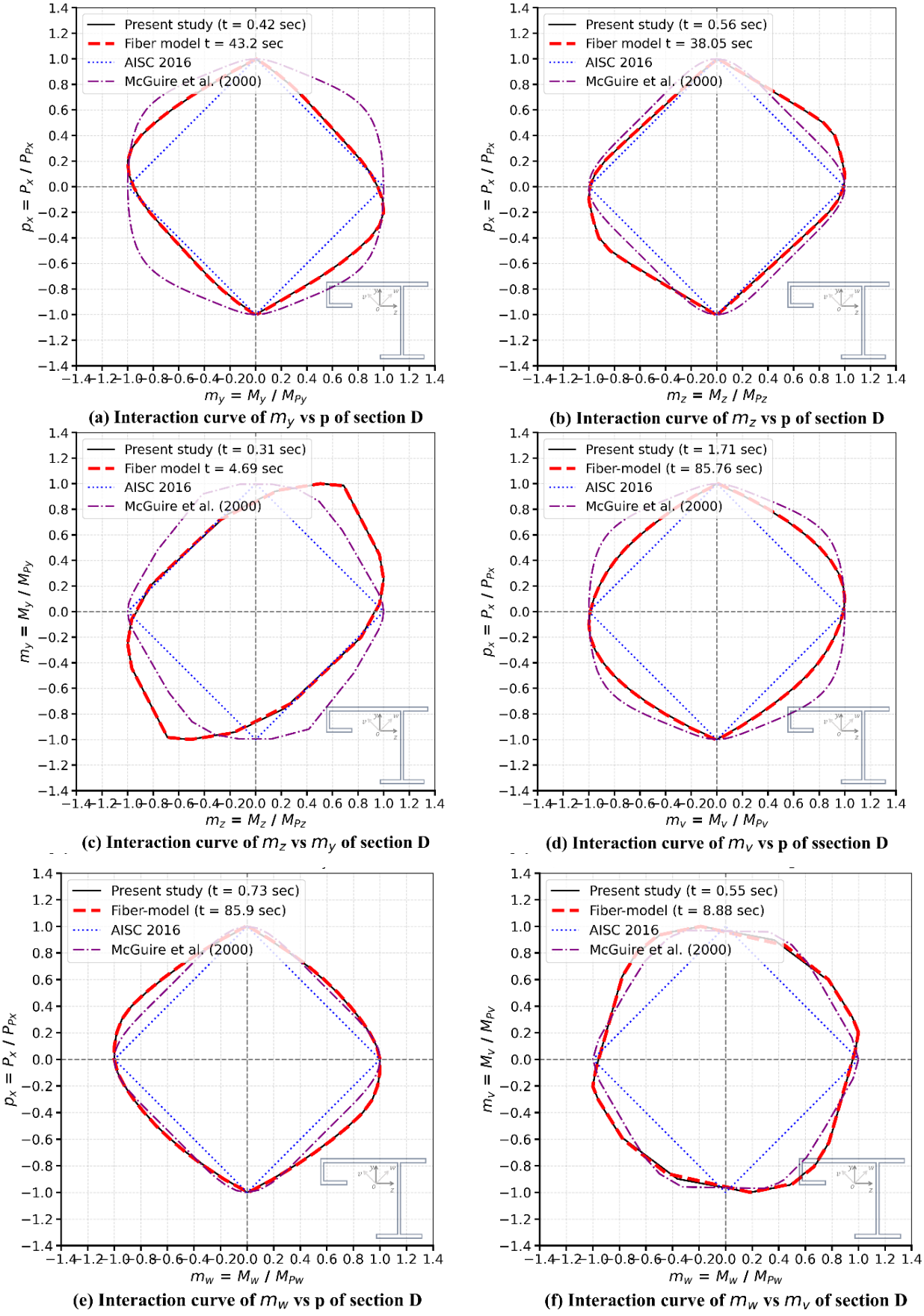

Fig. 11 Comparison results for the yield surface of section D

5.3. Example 3 – Validation of moment-thrust-curvature calculation

In this example, the moment-thrust-curvatures of three different sections (Fig. 12) are investigated to evaluate the accuracy and validity of the proposed method GSE. Similar to the previous example, three Gauss points are used along the thickness and seven along the length of each segment. The sections are analyzed using a bi-linear steel material model with Young's modulus of 200 GPa. Moment-curvature curves under different axial loads (0, 0.1Py, 0.2Py, 0.4Py, 0.6Py, and 0.8Py, with Py denoting the cross-sectional axial capacity) are provided. The comparative results are given in Figs. 13-15, where M_y and φ_y, indicate the initial yield moment and curvature, respectively. Results from the fiber-based method introduced by Chen et al. [11] and SE::MC [31] serve as the benchmark. In addition, results from the closed-form solutions introduced by Chen and Atsuta [32] for I-sections are also provided in Fig. 13.

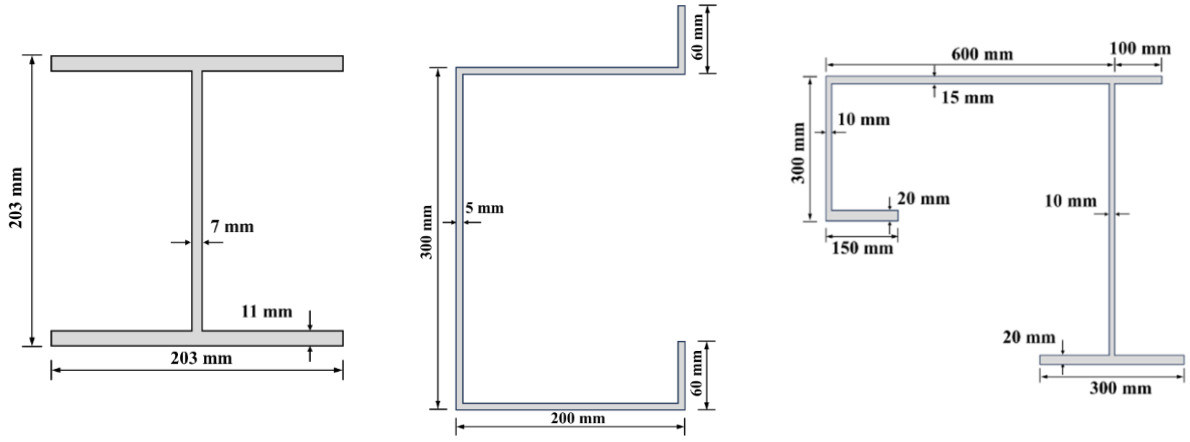

(a) W8x31 **(b) Lipped channel section** **(c) Irregular open section**

Fig. 12 The dimensions of the analyzed sections

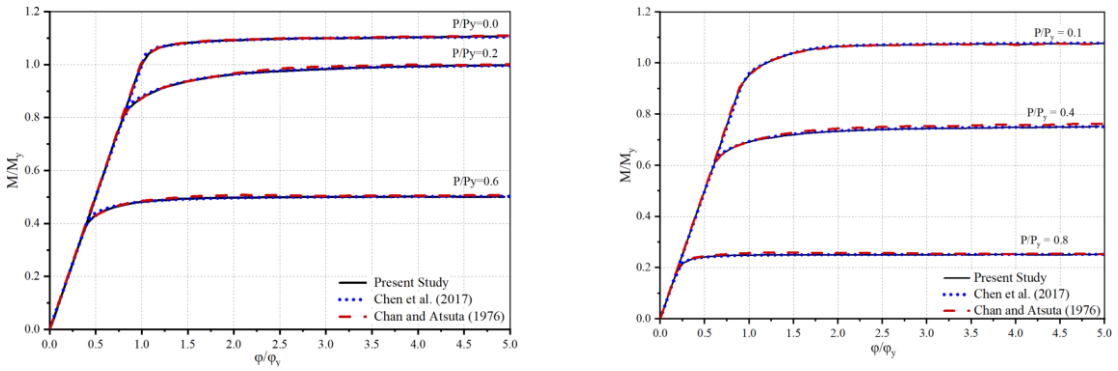

(a) P/Py = 0.0, 0.2, and 0.6 **(b) P/Py = 0.1, 0.4, and 0.8**

Fig. 13 Moment-thrust-curvatures of W8x31

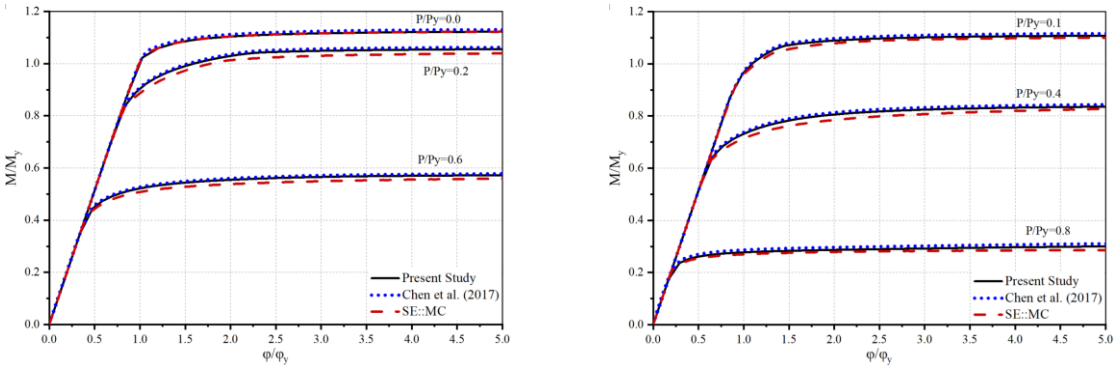

(a) P/Py = 0.0, 0.2, and 0.6 **(b) P/Py = 0.1, 0.4, and 0.8**

Fig. 14 Moment-thrust-curvatures of the lipped channel section

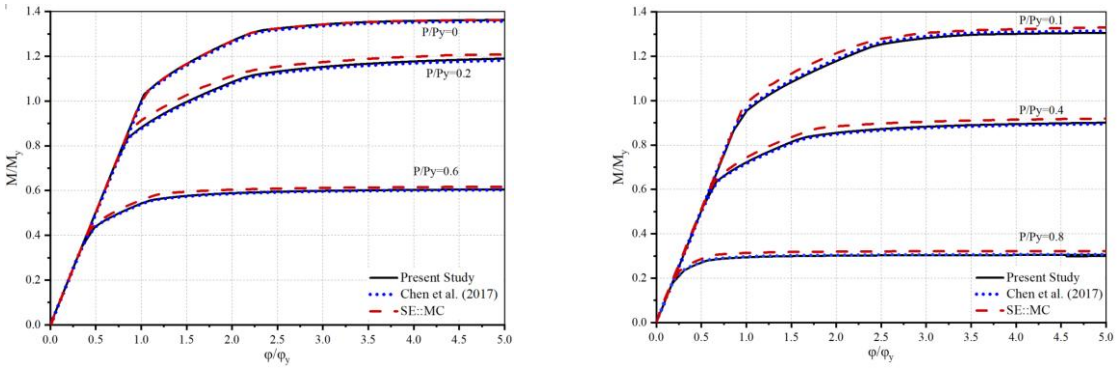

(a) P/Py = 0.0, 0.2, and 0.6 **(b) P/Py = 0.1, 0.4, and 0.8**

Fig. 15 Moment-thrust-curvatures of the irregular open section

Table 7
The computational time for fibre-based and proposed model

Section	P/Py	Fiber-based model (sec.)	Present Study (sec.)	Time reduction
(a) W8x31	0.0	2.03	0.43	78.8%
	0.1	1.58	0.46	70.9%
	0.2	2.71	0.98	63.8%
	0.4	2.17	0.72	66.8%
	0.6	3.02	1.71	43.4%
	0.8	2.86	1.21	57.7%
(b) Lipped channel section	0.0	1.93	0.51	73.6%
	0.1	1.53	0.52	66.0%
	0.2	2.39	0.96	59.8%
	0.4	2.15	0.79	63.3%
	0.6	2.89	1.61	44.3%
	0.8	2.21	1.46	33.9%
(c) Irregular open section	0.0	1.78	0.56	68.5%
	0.1	1.97	0.63	68.0%
	0.2	2.13	0.83	61.0%
	0.4	2.47	0.78	68.4%
	0.6	2.92	1.21	58.6%
	0.8	3.04	1.04	65.8%

Note: timings were obtained on the same workstation under identical software settings

The moment-thrust-curvatures obtained from the proposed method using GSE closely matched those from the fiber-based model using less computational time (Table 7). Based on these results, the proposed method using GSE has been demonstrated to be highly efficient, accurate, and reliable for the moment-thrust-curvature generation of arbitrary-shaped steel sections.

6. Conclusion

This paper proposes a Gaussian segmental element (GSE) framework for efficient cross-sectional analysis of arbitrary-shaped steel sections. This method employs a mesh-free line-segment representation with Gaussian quadrature for stress integration and introduces a refined line-segment model with end eccentricities to address overlap issues in tree-type geometries and improve geometric representation. Complete formulations and numerical procedures are presented and implemented in MSASect2, enabling the calculation of cross-section properties, full yield surfaces, and moment–thrust–curvature relationships. Validation against established benchmarks demonstrates that the proposed approach can deliver accurate sectional responses for a range of open and closed, symmetric and nonsymmetric sections, while reducing the computational effort associated with conventional fiber discretization. Future work will focus on (i) extending the geometric modeling to curved boundaries via segment refinement strategies, (ii) developing adaptive rules for segment subdivision and Gauss-point selection for highly localized response, and (iii) incorporating more general torsion/warping property evaluation for cases where thin-walled assumptions are not appropriate, together with broader validations for additional section families and material models.

Acknowledgement

The work described in this paper was partially supported by grants from the Research Grants Council of the Hong Kong Special Administrative Region through the projects "INTACT: Intelligent tropical-storm-resilient system for coastal cities (T22-501/23-R)" and " Second-order direct analysis for the design of steel members with irregular cross-sections (PolyU/21E/15203121)". Additional support was provided by the Department of Civil and Environmental Engineering at The Hong Kong Polytechnic University through the project "Development of Next-generation Sustainable Steel Construction using Built-up CFS Members (G-UAP3)", The third author is grateful for financial support from Mansoura University research unit for the project “Solar Energy Storage System Using a Medium of Sustainable Geopolymer Concrete” (MU-Eng-22-15).

References

[1] P. Waldron, "Sectorial properties of straight thin-walled beams," *Computers & Structures,* vol. 24, no. 1, pp. 147-156, 1986/01/01/ 1986. doi: https://doi.org/10.1016/0045-7949(86)90344-5

[2] Y. Chai Hong and S. V. Acra, "Cross-sectional properties of thin-walled multi-cellular section," *Computers & Structures,* vol. 22, no. 1, pp. 53-61, 1986/01/01/ 1986. doi: https://doi.org/10.1016/0045-7949(86)90084-2

[3] T. J. Li, S. W. Liu, and S. L. Chan, "Cross-sectional analysis of arbitrary sections allowing for residual stresses," *Steel and Composite Structures,* vol. 18, no. 4, pp. 985-1000, 2015.

[4] S. Abdelmageed and T. Zayed, "A study of literature in modular integrated construction - Critical review and future directions," *Journal of Cleaner Production,* vol. 277, p. 124044, 2020/12/20/ 2020. doi: https://doi.org/10.1016/j.jclepro.2020.124044

[5] X. Du and J. F. Hajjar, "Three-dimensional nonlinear mixed 6-DOF beam element for thin-walled members," *Thin-Walled Structures,* vol. 164, p. 107817, 2021/07/01/ 2021. doi: https://doi.org/10.1016/j.tws.2021.107817

[6] W. McGuire, a. R. H. Gallagher, and R. D. Ziemian, *Matrix Structural Analysis, 2nd Edition (Faculty Books. 7.)*. 2000.

[7]S.-W. Liu, Y.-P. Liu, and S.-L. Chan, "Advanced analysis of hybrid steel and concrete frames: Part 1: Cross-section analysis technique and second-order analysis," *Journal of Constructional Steel Research,* vol. 70, pp. 326-336, 2012/03/01/ 2012. doi: https://doi.org/10.1016/j.jcsr.2011.09.003

[8] L. Chen, W.-L. Gao, S.-W. Liu, R. D. Ziemian, and S.-L. Chan, "Geometric and material nonlinear analysis of steel members with nonsymmetric sections," *Journal of Constructional Steel Research,* vol. 198, p. 107537, 2022/11/01/ 2022. doi: https://doi.org/10.1016/j.jcsr.2022.107537

[9] L. Duan, J. T. Loh, and W. F. Chen, "Moment-Curvature Relationships for Dented Tubular Sections," *Journal of Structural Engineering,* vol. 119, no. 3, pp. 809-830, 1993/03/01 1993. doi: 10.1061/(ASCE)0733-9445(1993)119:3(809)

[10] A. Liew, L. Gardner, and P. Block, "Moment-Curvature-Thrust Relationships for Beam-Columns," *Structures,* vol. 11, pp. 146-154, 2017/08/01/ 2017. doi: https://doi.org/10.1016/j.istruc.2017.05.005

[11] L. Chen, S. W. Liu, and S. L. Chan, "Divergence-free algorithms for moment-thrust-curvature analysis of arbitrary sections," *Steel and Composite Structures,* vol. 25, pp. 557-569, December10 2017 2017.

[12] M. Mohareb and F. Nowzartash, "Exact Finite Element for Nonuniform Torsion of Open Sections," *Journal of Structural Engineering,* vol. 129, no. 2, pp. 215-223, 2003/02/01 2003. doi: 10.1061/(ASCE)0733-9445(2003)129:2(215)

[13] K. Saadé, B. Espion, and G. Warzée, "Discussion of “Exact Finite Element for Nonuniform Torsion of Open Sections” by Magdi Mohareb and Farhood Nowzartash," *Journal of Structural Engineering,* vol. 130, no. 9, pp. 1420-1420, 2004/09/01 2004. doi: 10.1061/(ASCE)0733-9445(2004)130:9(1420)

[14] M. Mohareb and F. Nowzartash, "Closure to “Exact Finite Element for Nonuniform Torsion of Open Sections” by Magdi Mohareb and Farhood Nowzartash," *Journal of Structural Engineering,* vol. 130, no. 9, pp. 1420-1421, 2004/09/01 2004. doi: 10.1061/(ASCE)0733-9445(2004)130:9(1420.2)

[15] O. Bourihane, A. Ed-dinari, B. Braikat, M. Jamal, F. Mohri, and N. Damil, "Stability analysis of thin-walled beams with open section subject to arbitrary loads," *Thin-Walled Structures,* vol. 105, pp. 156-171, 2016/08/01/ 2016. doi: https://doi.org/10.1016/j.tws.2016.04.008

[16] A. Elkaimbillah, B. Braikat, F. Mohri, and N. Damil, "A one-dimensional model for computing forced nonlinear vibration of thin-walled composite beams with open variable cross-sections," *Thin-Walled Structures,* vol. 159, p. 107211, 2021/02/01/ 2021. doi: https://doi.org/10.1016/j.tws.2020.107211

[17] G. J. Hancock and K. J. Rasmussen, "Formulation and Implementation of General Thin-Walled Open-Section Beam-Column Elements in Opensees (No. R961)," 2016.
[18] Rinchen, G. J. Hancock, and K. J. R. Rasmussen, "Geometric and material nonlinear analysis of thin-walled members with arbitrary open cross-section," *Thin-Walled Structures,* vol. 153, p. 106783, 2020/08/01/ 2020. doi: https://doi.org/10.1016/j.tws.2020.106783
[19] L. Chen, H.-Y. Zhang, S.-W. Liu, and D. Ziemian Ronald, "Efficient Line-Element Method for the Second-Order Analysis of Steel Members with Nonsymmetric Thick-Walled Cross Sections," *Journal of Structural Engineering,* vol. 150, no. 2, p. 04023226, 2024/02/01 2024. doi: 10.1061/JSENDH.STENG-12543
[20] S.-W. Liu, W.-L. Gao, and R. D. Ziemian, "Improved line-element formulations for the stability analysis of arbitrarily-shaped open-section beam-columns," *Thin-Walled Structures,* vol. 144, p. 106290, 2019/11/01/ 2019. doi: https://doi.org/10.1016/j.tws.2019.106290
[21] Hou, Yong, Junying Min, Nan Guo, Jianping Lin, John E. Carsley, Thomas B. Stoughton, Heinrich Traphöner, Till Clausmeyer, and A. Erman Tekkaya. "Investigation of evolving yield surfaces of dual-phase steels." *Journal of Materials Processing Technology,* vol. 287, p. 116314, 2021/01/01 2021. doi: https://doi.org/10.1016/j.jmatprotec.2019.116314
[22] Skordeli, M-AA, and C. D. Bisbos. "Limit and shakedown analysis of 3D steel frames via approximate ellipsoidal yield surfaces." *Engineering Structures*, vol. 32, no. 6, p. 1556-1567, 2010/06/01 2010. doi: https://doi.org/10.1016/j.engstruct.2010.02.004
[23] Hoang, Hieu Nghia, Quoc Anh Vu, and Manh Hien Nghiem. "An Approximation of Yield Surface for Doubly Symmetrical Sections of Steel Structures." *Periodica Polytechnica Civil Engineering,* vol. 69, no. 1, P. 321-332, 2025. doi:https://doi.org/10.3311/PPci.36589
[24] Vu, Anh Q., Nghia H. Hoang, and Hien M. Nghiem. "An efficient method for yield and failure surfaces of the steel i-section." *Advanced Steel Construction*, vol. 16, no. 3, P. 246-254, 2020/09/01 2020. doi: https://doi.org/10.18057/IJASC.2020.16.3.6
[25] Rakici, Salih, and Fatmir Menkulasi. "Moment curvature response of composite UHPC filled hollow structural steel cross-sections." *Engineering Structures*, vol. 294, P. 116728, 2023/11/01 2023. doi: https://doi.org/10.1016/j.engstruct.2023.116728
[26] Chiorean, Cosmin G. "A computer method for moment-curvature analysis of composite steel-concrete cross-sections of arbitrary shape." Engineering Structures and Technologies, vol. 9, no. 1, P. 25-40. 2017/01/02 2017, doi: https://doi.org/10.3846/2029882X.2017.1299969.
[27] Sun, Zeyang, Yang Yang, Wenlong Yan, Gang Wu, and Xiaoyuan He. "Moment-curvature behaviors of concrete beams singly reinforced by steel-FRP composite bars." *Advances in Civil Engineering*, vol. 1,P. 1309629. 2017.doi: https://doi.org/10.1155/2017/1309629
[28] Abdallah, Maha Hussein, Hamdy M. Mohamed, Radhouane Masmoudi, and Ahmed Moussa. "Analytical modeling of moment-curvature behavior of steel and CFRP RC circular confined columns." *Composite Structures*, vol. 189, p. 473-487, 2018/04/01 2018, doi: https://doi.org/10.1016/j.compstruct.2018.01.110.
[29] Montuori, Rosario, and Vincenzo Piluso. "Analysis and modelling of CFT members: moment curvature analysis." *Thin-Walled Structures*, vlo. 86, p. 157-166. 2015/01/01 2015. doi: https://doi.org/10.1016/j.tws.2014.10.010
[30] Rodriguez-Gutierrez, J. A., and J. Dario Aristizabal-Ochoa. "Bending moment-axial force-curvature interactions for metal beam-column sections." *Structures*, vol. 10, p. 139-146. 2017/05/01 2017. doi: https://doi.org/10.1016/j.istruc.2017.03.003
[31] T. J. R. Hughes and W. K. Liu, "Nonlinear finite element analysis of shells: Part I. three-dimensional shells," *Computer Methods in Applied Mechanics and Engineering,* vol. 26, no. 3, pp. 331-362, 1981/06/01/ 1981. doi: https://doi.org/10.1016/0045-7825(81)90121-3
[32] E. Spacone, F. C. Filippou, and F. F. Taucer, "FIBRE BEAM–COLUMN MODEL FOR NON-LINEAR ANALYSIS OF R/C FRAMES: PART I. FORMULATION," *Earthquake Engineering & Structural Dynamics,* vol. 25, no. 7, pp. 711-725, 1996/07/01 1996. doi: https://doi.org/10.1002/(SICI)1096-9845(199607)25:7<711::AID-EQE576>3.0.CO;2-9
[33] N. R. B. K. Raju and J. Nagabhushanam, "Nonlinear structural analysis using integrated force method," *Sadhana,* vol. 25, no. 4, pp. 353-365, 2000/08/01 2000. doi: 10.1007/BF03029720
[34] C. M. Tiago and V. M. A. Leitão, "Application of radial basis functions to linear and nonlinear structural analysis problems," *Computers & Mathematics with Applications,* vol. 51, no. 8, pp. 1311-1334, 2006/04/01/ 2006. doi: https://doi.org/10.1016/j.camwa.2006.04.008
[35] E. Parente Jr, G. V. Nogueira, M. Meireles Neto, and L. S. Moreira, "Material and geometric nonlinear analysis of reinforced concrete frames," *Revista IBRACON de Estruturas e Materiais,* vol. 7, 2014.
[36] L. Chen, A. H. A. Abdelrahman, S.-W. Liu, D. Ziemian Ronald, and S.-L. Chan, "Gaussian Beam–Column Element Formulation for Large-Deflection Analysis of Steel Members with Open Sections Subjected to Torsion," *Journal of Structural Engineering,* vol. 147, no. 12, p. 04021206, 2021/12/01 2021. doi: 10.1061/(ASCE)ST.1943-541X.0003185
[37] W.-L. Gao, A. H. A. Abdelrahman, S.-W. Liu, and R. D. Ziemian, "Second-order dynamic time-history analysis of beam-columns with nonsymmetrical thin-walled steel sections," *Thin-Walled Structures,* vol. 160, p. 107367, 2021/03/01/ 2021. doi: https://doi.org/10.1016/j.tws.2020.107367
[38] S.-W. Liu, R. D. Ziemian, L. Chen, and S.-L. Chan, "Bifurcation and large-deflection analyses of thin-walled beam-columns with non-symmetric open-sections," *Thin-Walled Structures,* vol. 132, pp. 287-301, 2018/11/01/ 2018. doi: https://doi.org/10.1016/j.tws.2018.07.044
[39] S. W. Liu and R. D. Ziemian, "MSASect2 - Matrix Structural Analysis Software for Arbitrary Cross-sections. Retrieved from http://www.msasect.com," ed, 2023.
[40] AISC, Specifications for Structural Steel Buildings ANSI/AISC 360-16, American Institute of Steel Construction, Chicago, C. American Institute of Steel Construction. 2016.
[41] Structure Express, "SE::MC – Moment Curvature Analysis (V2015.06.01)", 2024, software available at http://structurexpress.com/
[42] W. F. Chen. and and T. Atsuta, *Theory of Beam Columns: In-Plane Behavior and Design*. Ross Publishing, 1977.